Final Report for NASA Grant NAGW-4797

The Shoemaker-Levy 9/Jupiter Impact: Auroral and High Energy Processes

Submitted in Response to
NASA Research Announcement NRA 95-OSS-03

Original Funding period: September 1, 1995 to August 31, 1996
Extended at No Additional Cost to September 30, 1997

Principal Investigator: Michael R. Combi

Space Physics Research Laboratory
The University of Michigan
2455 Hayward Street
Ann Arbor, MI 48109-2143\

Co-Investigators: Rainer Bauske, University of Michigan (replacing Ronald Miller)
J. Hunter Waite, Southwest Research Institute
John T. Clarke, University of Michigan
Gilda E. Ballester, University of Michigan

Abstract

During the impact of comet Shoemaker-Levy 9 fragment K on Jupiter various observers detected aurora-like emissions near to the impact region as well as in the other hemisphere at approximately magnetic conjugate positions equatorward of auroral latitudes. A number of generation mechanisms were suggested, but investigations of their significance have been hampered by a lack of knowledge about the Jovian internal magnetic field, the exact timing and the geometry of the impact and emission sites. We use a recently developed model of the internal magnetic field, high time resolution calculations of the fragment K trajectory and images from the Hubble Space Telescope Wide Field Planetary Camera 2 with advanced processing to constrain possible mechanisms. It turns out that the impact location is surrounded by two regions of enhanced far ultraviolet emissions. The southern region is partly in the projection area of two brighter emission regions observed on the northern hemisphere and approximates the shape of the projection. The latter regions as well as the southern region are crossed by the magnetic footprints of the approaching fragment which correspond to heights of about 2723 to 10691 km for the southern region. For the emission region northward of the impact location and for the impact location itself there is no enhanced emission found at the conjugate locations on the other hemisphere. Amalthea's footprint is located in the gap between the two northern hemispheric emission regions. We suggest, that Amalthea may be responsible for a disturbance which scatters particles coming from the southern hemispheric emission regions onto field lines which connect to the northern emission regions at slightly higher latitudes. Shock acceleration connected with bouncing of the ejecta may be responsible for the existence of the northern hemispheric emission regions.

I. Introduction

The collision of comet Shoemaker-Levy 9 with Jupiter in July of 1994 represented one of the most spectacular transient natural phenomena ever to have been observed in the solar system. An impressive armada of observational resources -- ground-based telescopes, and orbiting and interplanetary spacecraft -- was assembled to collect data regarding all aspects of the event, with the US efforts largely supported by NASA and NSF. The study of the response of Jupiter's ionosphere and magnetosphere to the encounter of the comet and its impact is an important element of the overall event. Its study also presents an opportunity for us to further our understanding of the "normal" state. With this in mind a proposal was submitted in response to NASA Research Announcement NRA 95-OSSA-03 to bring together observations supported by NASA with an established base of theoretical expertise supported in the past by NASA and NSF, for Jupiter and Earth ionosphere/magnetosphere studies and for studies of the interaction of Jupiter's magnetosphere with Io's atmosphere in order to address a suite of observations which indicate that coupled ionospheric/magnetospheric processes were associated with the encounter and impact of the comet with Jupiter.

To accomplish this we brought together a team composed of investigators responsible for some important impact datasets and experienced with ionospheric and auroral models of Jupiter's upper atmosphere and magnetosphere and with analogous areas of study associated with the Earth's ionosphere and magnetosphere. This study focused in particular on ultraviolet imaging data taken by the Hubble Space Telescope [Clarke et al., 1995] ultraviolet spectra from IUE [Ballester et al., 1995] and X-ray emission data taken by the ROSAT (Röntgensatellit) [Waite et al., 1995]. Of course, other relevant complementary published observations were also to be incorporated. The project was funded in two parts, one under the direction of this Principal Investigator at the University of Michigan, and another under the direction Dr. J. Hunter Waite at the Southwest Research Institute (SWRI). The latter efforts at SWRI concentrated on the interpretation of the ROSAT measurements and are reported separately by them. In this report we will discuss the progress and current status of the work undertaken at the University of Michigan alone.

II. Background

By 22 July 1994 the 21 individual nuclei and their accompanying comae of comet Shoemaker-Levy 9 had entered the inner magnetosphere of Jupiter and impacted near latitude 44° S in its atmosphere passing at a zenith angle of about 45° and a speed of ~60 km/s just over the limb

as viewed from Earth. Various phenomena associated with the nuclei impacting Jupiter were observed in various wavelengths (X-ray to radio), monitoring the initial flash, the rise of the fireball, and the ballistic falling back of the cooling cloud (aerosols and gas) by numerous groups [see May 15, 1995 GRL special issue and Volume 267, 1995, of Science]. In addition to atmospheric phenomena directly associated with the impacts, ionospheric and magnetospheric phenomena associated with both the impacts themselves as well as the passing of the fragment nuclei and their associated comae through the magnetosphere have been observed [Clarke et al., 1995; De Pater et al., 1995; Prangé et al., 1995; Waite et al., 1995; Miller et al. 1995]. A number of scenarios for such interactions had been predicted before the impacts [Cravens, 1994; Dessler and Hill, 1994a; Cevalier and Sarazin 1995].

The Wide Field Planetary Camera 2 (WFPC 2) and the Faint Object Camera (FOC) were used by Clarke et al. [1995] to monitor such activity. WFPC 2 was used to construct image sets using filter F160BW, having a bandpass of 1150 to 2100 Å, and filters F160BW + F130LP, having a combined bandpass of 1300 to 2100 Å. F130LP is a long pass filter which excludes hydrogen Lyman-alpha. The FOC was used to construct image sets using combinations of filters F152M and F175W (theoretical bandpass of about 1460 to 1670 Å), for the purpose of separating the long wavelength portion of the auroral H_2 Lyman band emission. Note that the effective bandpass for the impact sites may be shifted to slightly longer wavelength due to the shape of Jupiter's reflection spectrum. Auroral activity was found in the northern hemisphere in the vicinity of the magnetic conjugate point of the K impact in images that were taken 47 and 57 minutes after the impact, and shown in Figure 1. Variable auroral activity was observed inside the southern hemisphere auroral oval in images taken just before the Q1 and Q2 impacts and has been geometrically (but not yet physically) modeled in terms of the comet fragments and comae passing through auroral oval magnetic flux tubes by Prangé et al. [1995].

Several processes which could possibly be responsible for the UV emissions in the hemisphere conjugate to the impact had been considered by Clarke et al. [1995]. Clarke et al. suggested that, in analogy with processes at the Earth [Gombosi and Nagy, 1989], high temperatures associated with the impact site could have produced enough plasma constrained by the magnetic field to have flowed from the southern hemisphere to the north causing auroral activity there. Another process could have been wave activity (whistler or Alfvén) propagating along the field lines presumably through wave particle interaction [Waite et al., 1994]. Lastly, the thermospheric winds moving away from the impact site could produce field-aligned currents that would have closed in the conjugate ionosphere (the north) producing the auroral emissions [Dessler and Hill, 1994b]. It is was apparent that these, or possibly other scenarios, might have

been possible explanations, however, only detailed modeling of such events could provide an adequate answer. This is true equally for the auroral activity in the northern (conjugate) hemisphere as well as for auroral oval activity associated with pre-impact passage of fragments and associated comae or post-impact plume material connected through magnetic flux tubes.

The IUE campaign to observe the Shoemaker-Levy 9 impact with Jupiter included several independent investigations (1) albedo changes of the upper atmosphere with time, (2) changes in the auroral emissions, (3) Jupiter plasma torus observations, and (4) direct observations at the limb of the impact site during the impacts themselves. Ballester et al. [1995] described the last of these which are relevant to the modeling studies undertaken here. The H_2 Lyman- and Werner-bands (1230-1620 Å), H-Ly-α, C 1657 Å and possibly Al^+ 1671 Å emissions have been identified in 20 minute spectra centered around the impact time. They concluded that the emissions could result from either plasma processes generated by the impacts, from resonant and fluorescent scattering by the upper atmosphere and ablated cometary material, or from thermal emission by the hot entry shock and/or the early fireball. There were predictions of possible UV emissions produced during various stages of the impact including the shock produced by the entry fragment, the explosion shock and the hot fireball [Chevalier and Sarazin, 1994; Boslough et al., 1994; Kellogg, 1994]. As in the cases of the previous data sets, detailed modeling would have been required to understand the observations and decide which are the important mechanisms responsible for the observed emissions. Such analysis would also yield a clearer picture of the basic physical nature and evolution of the entire impact process.

The original plan for this project was to apply a number of models, developed to understand ionospheric and inner-magnetospheric processes in the vicinity of the Earth, in order to test the various suggested processes and compare with the observations. The major modeling tools were developed through the efforts of one of the original Co-Investigators, Dr. Ronald Miller, in collaboration with the Principal Investigator [Miller and Combi 1994; Miller et al. 1995]. Near the beginning of the project Dr. Miller decided to leave space research at the University of Michigan and to pursue an industrial research career. In response to this, as well as other research needs in our larger research group, we brought in a postdoctoral research fellow, Dr. Rainer Bauske, to take on the role of Dr. Miller. Because of the unavoidable delays in this process, we requested and received a no-cost time extension and carried out most of the research during the second year.

Shortly after beginning the work on this project we obtained some new (rudimentary) image projection software for study of HST images of Jupiter from our Co-Investigator Dr. Clarke, which lead to some fundamentally important and startling new discoveries about the

primary data set upon which the research program was based. It was clear that an alternate approach to understanding these data was needed to completely reevaluate the basic observational evidence, and only then reconsider the previously suggested, as well as new possible mechanisms for the auroral phenomena. The following section of this report will describe our findings.

III. Progress of Research

III.A Observations

Clarke et al. (1995) reported observations at far-ultraviolet (FUV) wavelengths done with the Hubble Space Telescope (HST) Wide Field Planetary Camera 2 (WFPC2). This group observed atypical auroral emissions (1150 to 2100 Å and 1300 to 2100 Å) at two northern locations from (jovigraphic latitude, System III longitude) +51°, 257° to +56°, 277° and +56°, 238° to +56°, 256° in two images obtained 47 and 57 minutes after the impact of the K fragment of comet Shoemaker-Levy 9 on Jupiter. They also detected 'fainter but significant' emissions between -54°, 275° and -52°, 280°, just south of the impact cite, and noted that these came from an area with unusual FUV absorption from the impact, so that the north-south ratio of auroral excitation may have been closer to unity than observed. All emissions decreased in time between the two images. Using the O6 model of Connerney (1992), they showed roughly a magnetic connection between the lower-latitude northern and the southern emission region. Assuming the K-impact at -43.8°, 279° they were unable to detect any emission at its northern conjugate point, +38°, 269°.

McGregor et al. (1996) used the near-infrared Cyrogenic Array Spectrometer / Imager (CASPIR) on the Australian National University 2.3-m telescope at Sliding Spring Observatory, Australia, to record lightcurves at 2.34 μm and images at narrow bands with central wavelengths ranging from 1.1 to 48 μm of the impacts of various fragments. They obtained a lightcurve of the K-event from about 10 minutes before until 21 minutes after impact time (10:24:13 UT on July 19, 1994) which shows among other features precursor emission starting about 3.5 minutes before impact and the main brightening starting about 6 minutes after the impact. These times are in agreement with observations from other groups, e.g., Watanabe et al. (1995) who measured the lightcurve at 2.35 μm with a higher time resolution (10 s). McGregor et al. (1996) also reported transient auroral emission seen on 3.3 - 3.99 μm images following the G, K, R, and W impacts, especially an emission spot visible ~30 minutes after the K impact at about +55°, 250° but not seen again ~45 minutes later. The other emissions were observed at similar locations relative to the impact sites and, summarizing, at times from 20 minutes until about an hour after each impact,

lasting less than 45 minutes up to one hour. The relative intensities of these emissions support the idea of strong contributions from H_3^+ because strongest intensities occurred at 3.42 μm which is also observed for the jovian aurorae (Kim et al. 1991, Baron et al. 1991). Large rings seen in the 3 - 4 μm images around the G and K impact sites also belong to the most prominent effects observed on timescales shorter than about 3.5 h.

Ballester et al. (1995) obtained far-UV spectra (~1700 - 2000 Å) of the K, P2, and S impacts with the SWP camera of the International Ultraviolet Explorer (IUE). The impacts were observed for about 20 minutes centered on impact time. H_2 Lyman and Werner band (1230 - 1620 Å), H-Ly α emissions and emissions by Al^+ (1671 Å) and C (1657 Å) were identified, the latter two only tentatively. The H and H_2 emissions resembled a spectrum which is expected from collisional excitation by electrons if one accounts for significant absorption by CH_4, the main stratospheric component. Ballester et al. (1995) stated that their observations would agree with the decay time scale of the WFPC2 emissions or could accommodate stronger emissions near impact time. They argued about other excitation processes, leaving high altitude (bolide) line emission produced by shocked atmospheric and ablated gases (Chevalier and Sarazin, 1994) as another possible candidate. These emissions could have been observed between altitudes of ~830 km projected above the limb of the CH_4 homopause and 2000 km in height which is the maximum extension inferred by Chevalier and Sarazin (1994).

III.B Recent developments

Connerney et al. (1997) developed a model of Jupiter's magnetic field, the 'VIP 4 degree/order model', taking into account the distinct H_3^+ emission feature observed at the foot of the Io flux tube (Connerney et al., 1993) as well as *in situ* helium magnetometer measurements of Pioneer 10 and 11, the fluxgates on Pioneer 11, Voyager 1 and 2, and Ulysses. The H_3^+ emission feature is frequently observed whenever Io's phase allows the visibility of its footprint locations from earth (Clarke et al. 1996). The model uses (currently) 112 distinct observations from 1992 to 1996 which were done with the WFPC2 and the Faint Object Camera (FOC) on the HST and with the NSFCAM infrared camera of NASA's Infrared Telescope Facility (IRTF) on Mauna Kea, Hawaii. Most longitudes in the northern hemisphere and all longitudes in the southern hemisphere are covered by observations with errors estimated to be ±1-2° in latitude and ±2-15° in latitude depending on the proximity of the feature to the limb and on the image quality. On the northern hemisphere the region between 0° and 150° longitude is sparsely sampled. Due to their generalized inverse approach (for a description see Connerney, 1981), Connerney et al. (1997) could not give

standard deviations of their VIP 4 model, but they showed that calculated footprints are within the observational errors.

Chodas and Yeomans (1995) refined their orbit calculations by using observed impact times and by estimating and removing star catalog errors from all astrometic observations they used in the reduction of the fragment's positions. We use results from a high time resolution calculation of the fragment K's final approach kindly provided by Paul Chodas in order to determine which height region of its trajectory is connect to the far-UV emission regions.

Clarke et al. (1996) modeled the long wavelength disk component of Jupiter (1700 - 2100 Å) which is dominated by scattered solar continuum emission and subtracted it from the WFPC2 FUV images obtained between 05 / 19 / 1995 and 09 / 26 / 1995, which includes the images of the SL9 K fragment impact introduced above. The resulting images show the wavelength region from 1300 to 1700 Å (47 minutes past impact) and from 1150 Å to 1700 Å (57 minutes past impact). These ranges correspond to lower altitudes of the sampled atmospheric region from about 200 km (~ 0.1 mbar level) at 1700 Å due to C_2H_2 absorption up to 400 km (~ 10 μbar level) at 1450 Å due to increasingly strong CH_4 photoabsorption (Clarke et al., 1995, 1996). Above the impact site lower heights are difficult to determine due to increased heating and changing chemical conditions. For auroral emissions extending above the planetary limb, modeled ovals with base heights of 400 to 700 km in general give good fits to the far-UV observations.

III.C Image processing and magnetic mapping

We apply the VIP 4 model coefficients for Jupiter's internal magnetic field to trace various fieldlines in the impact and emission regions. For the longitude of the K impact our calculated locations deviate less than 0.5° in latitude and 1.1° in longitude from footprint locations of Amalthea, Io, Europa, and Ganymede derived with the 'full' VIP 4 model which includes the contribution of the current disc to the far magnetic field. In our calculations, we assumed that the optical surface of the disk has heights between 0 and 400 km. Differences in the overlay of calculated footprints on the images are small for the borders of this height range, even near to the limb.

Figure 1 updates Figure 3 of Clarke et al. (1995). It shows the subtracted images which are now overplotted by fieldlines from our VIP 4 model version. In the left image (47 minutes past impact, referred to as 'earlier' image), emissions are apparent north and south of the impact regions. In the later image the northern emission is gone and the other has faded, similar to the

emissions seen on the northern hemisphere. In addition, the final 20 minutes of the trajectory of the approaching fragment is plotted, calculated with time steps of one minute. The impact location is (jovigraphic latitude, longitude, height) -47.7°, 278.0°, 40.43 km and the impact time is July 19, 10:24:13 UTC. The exposure time was 400 s which leads to a smear of 4° in longitude due to the rotation of Jupiter.

These images were further processed with the help of a back-projection algorithm. In Figure 2a and b we rotated the viewpoint in order to get a better overview of the impact and northern emission regions. We projected footprints of Io (5.9 R_j) and Amalthea (2.54 R_j) from Connerney (1997) (given in jovicentric coordinates) down to the jovigraphic surface (here at 50 km height) and we additionally calculated and plotted footprints of the approaching fragment. The black texture near to the terminator is due to the fixed size of pixels in the back-projection algorithm. Several features are remarkable:

The impact location is surrounded by two regions of enhanced far ultraviolet emissions with the shape of a twice broken ring, extended to the south east. The southernmost emission region is crossed by the approaching fragment's footprints approximately in the middle. The corresponding height range of the fragment trajectory is from about 2723 to 10691 km. The emission region north of the impact was not reported by Clarke et al. (1995), although it is visible in the original image (Figure 3). The emission regions on the southern hemisphere are fainter than those on the northern hemisphere. The latter ones are located to both sides of the trajectory footprint path. Footprints of Amalthea are on the border of the northernmost emission region. The latitude position of these markings relative to the underlying image somewhat reflects assumptions about the base-height of the visible surface, but differences are small for base-heights between 0 and 400 km.

Two major questions emerge form these images: Where were Amalthea and its footprints at the times of impact and of the first image? Are projections of the northern hemispheric emission regions really contained in the southernmost emission region? For the following descriptions we name the emission regions from north to south, starting with N1 and N2 on the northern hemisphere, followed by S1, the region north of the impact and finally S2 south of it. Projected regions are named by " #' " where "#" is one of those names.

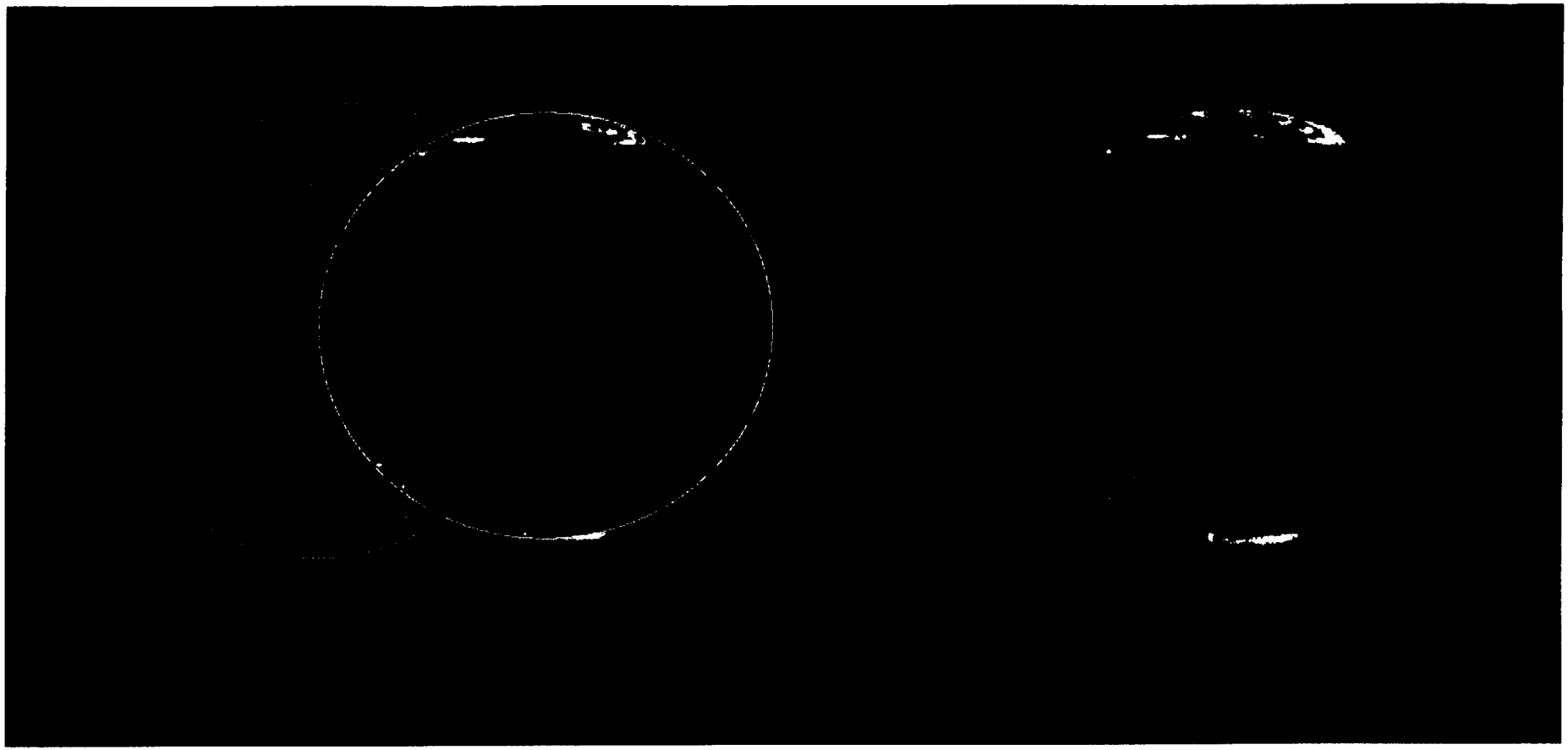

Figure 1
WFPC2 FUV images started at 11:07:17 UT (left) and 11:17:17 UT (right) with an exposure time of 400 s, thus centered about 47 and 57 min after the impact. The exposure time leads to a smear of 4° in longitude due to the rotation of Jupiter. The contribution of solar scattered continuum emission to the long wavelength disc component of Jupiter (1700 - 2100 Å) has been modeled and subtracted from the original images which sampled wavelength ranges of 1300 to 2100 Å (left) and 1150 to 2100 Å (right). Diamonds show the trajectory of the incoming fragment K with timesteps of one minute up to the impact location which is calculated as (latitude, longitude, height) -47.7°, 278.0°, 40.43 km on July 19, 10:24:13 UTC. Magnetic field lines starting at the impact site and in two emission regions on the northern hemisphere are modeled with the VIP 4 model.

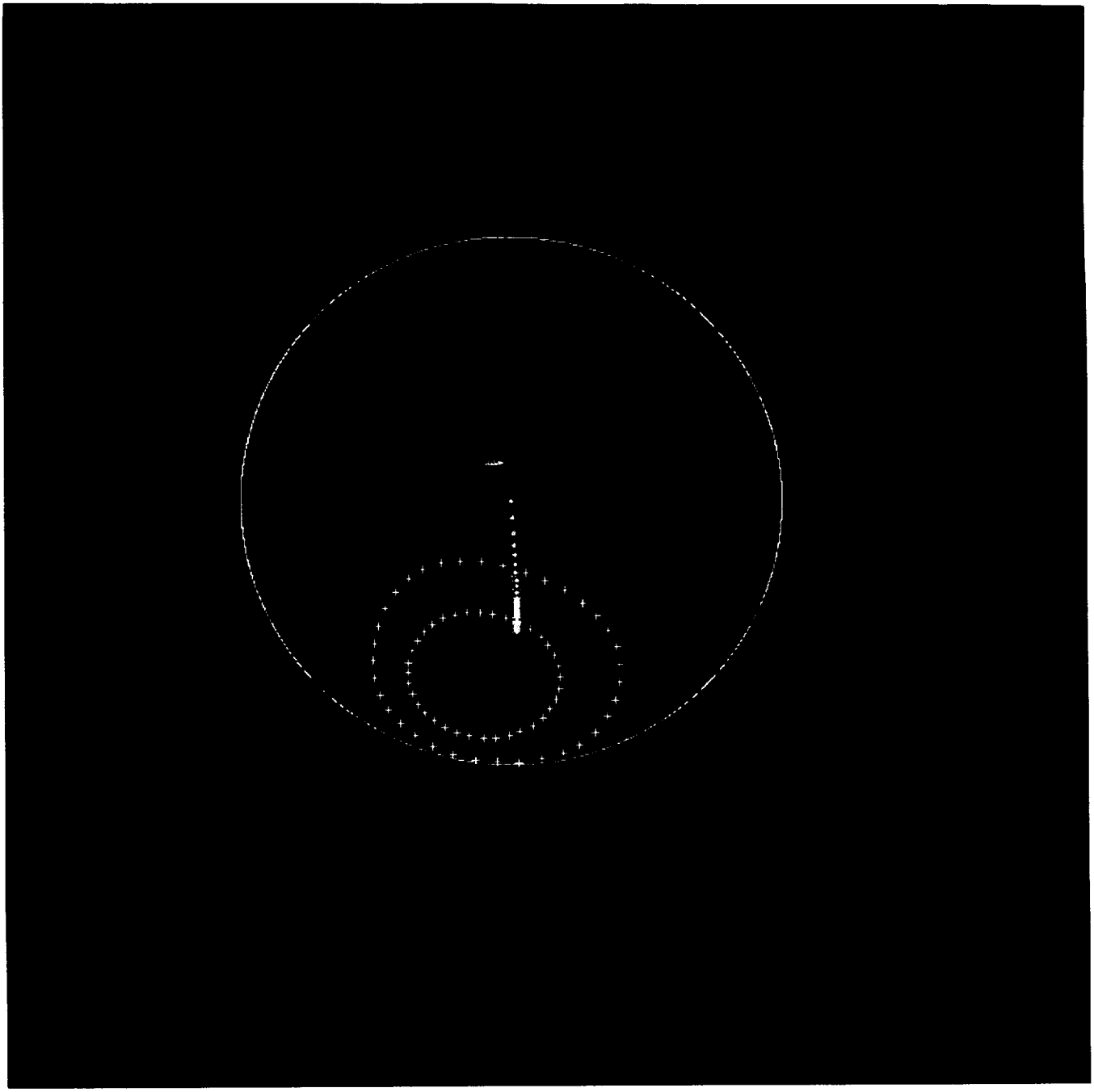

Figure 2a
Backprojections of the left image in Figure 1 (47 min a. I.) centered at (latitude, longitude) -47.7°, 278.0 (left) and 54.0°, 259.0 (right). Footprint locations of the fragment trajectory (stars, 1 min time steps) and of the satellites Amalthea (outer ring) and Io (inner Ring) are calculated for a jovigraphic height of 50 km. The black texture near to the terminator results from a fixed size of pixels at all longitudes. Io's footprint is visible south of the calculated footprints as a small separated emission feature. The deviation of the calculated position for 11:11 UTC is about 3° in longitude as well as in latitude.

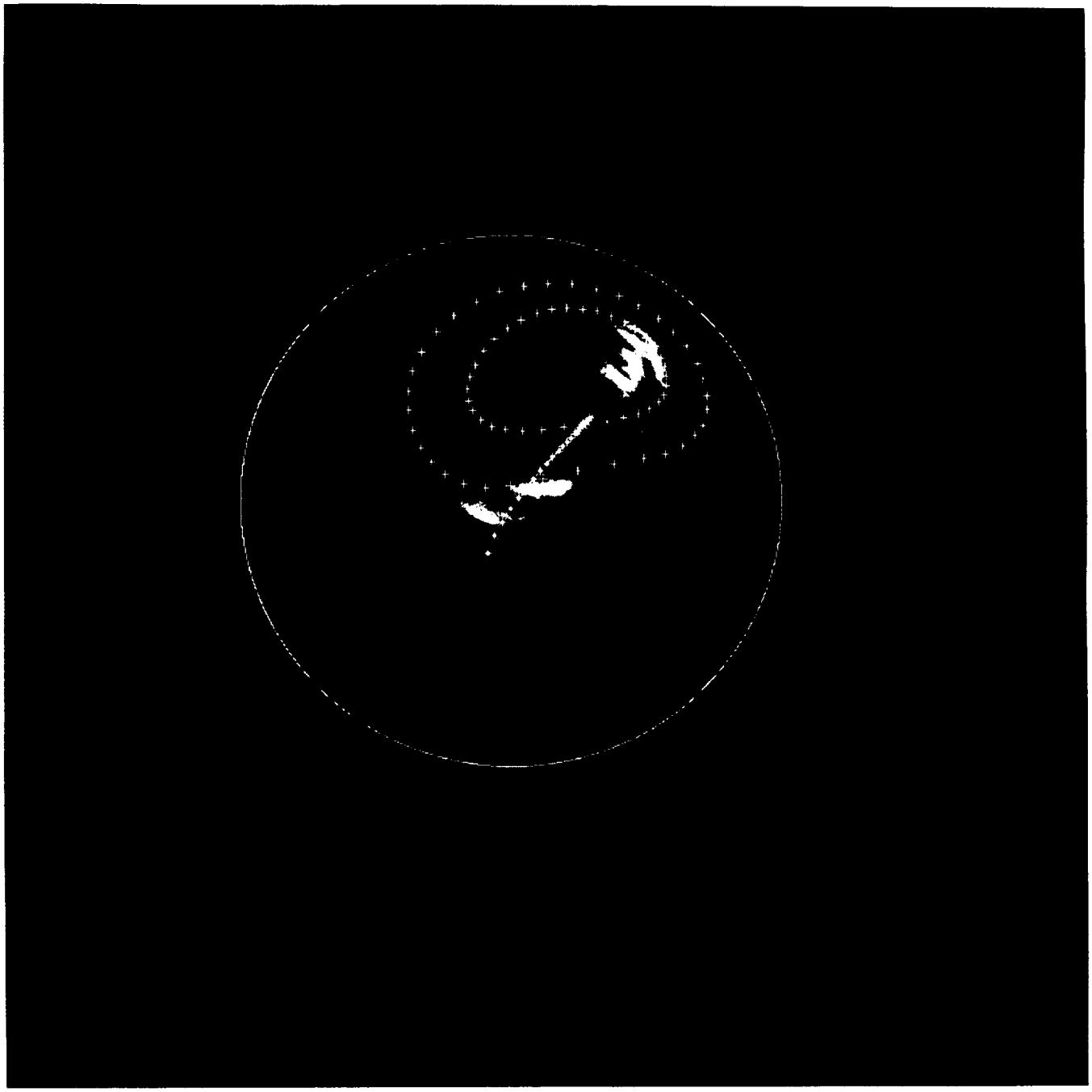

Figure 2b
See caption for Figure 2a.

Figure 3a
Zoomed part of Figure 2b, centered at 54.0°, 259.0. The emission boundaries were marked with stars for later use. A diamond shows the location of a hot spot observed by McGregor et al. (1996) about 30 minutes after the impact. The triangle and the 'X' show the positions of Amalthea's footprint at the times of the impact and at 11:11.

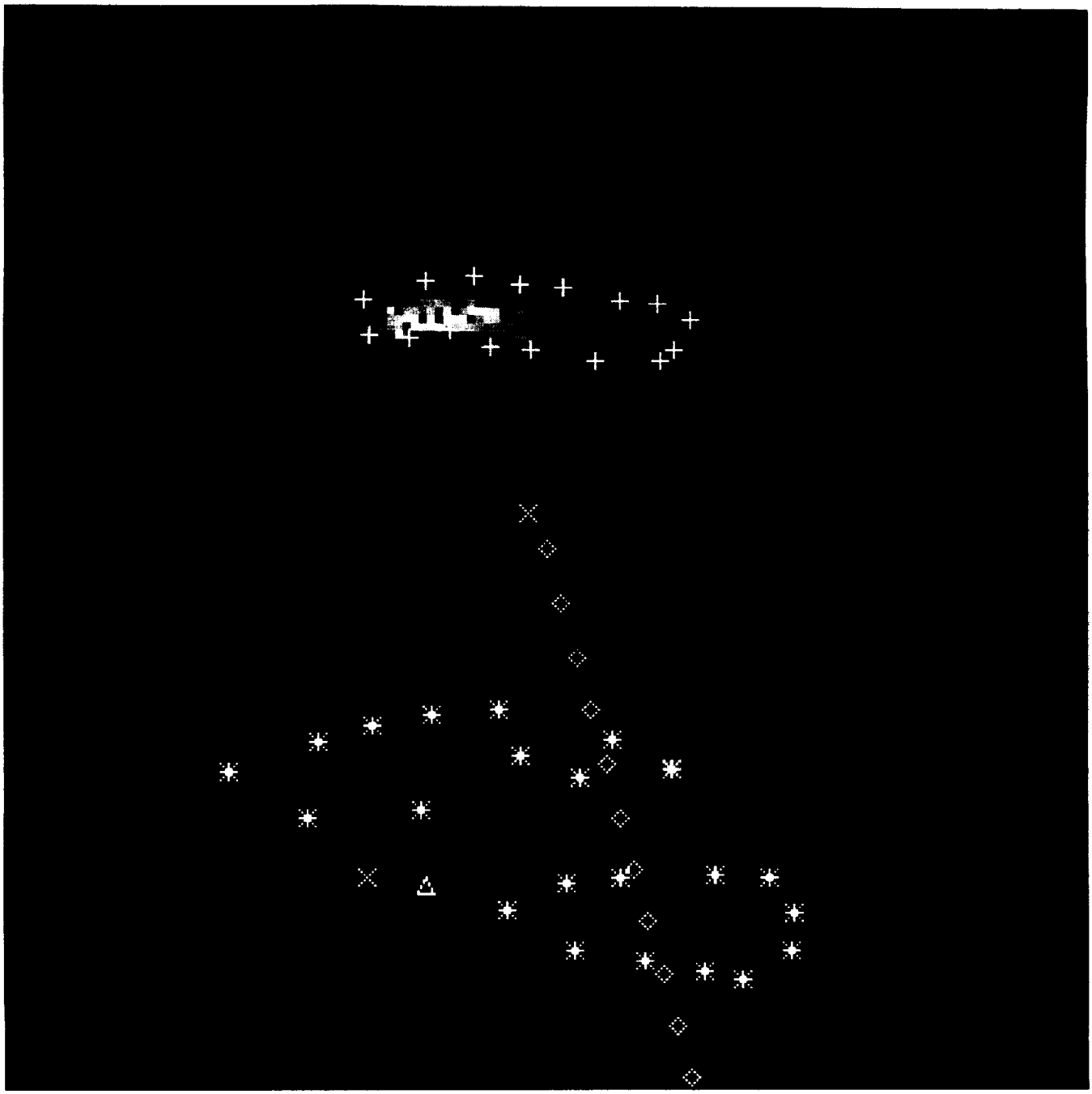

Figure 3b
Zoomed part of Figure 2a, centered at -47.7°, 278.0. Boundaries of the brightest parts in northern emission region are marked with crosses for later use. Stars show the magnetic footprints of marks from Figure 3a, diamonds mark the trajectory (not footprints!) of the incoming fragment. The cross in continuation of the trajectory markings is the averaged center position of the great rings observed by McGregor et al. (1996). Amalthea's footprints are shown as in Figure 3a. Note the circular shape of the emission region boundaries around the ring center.

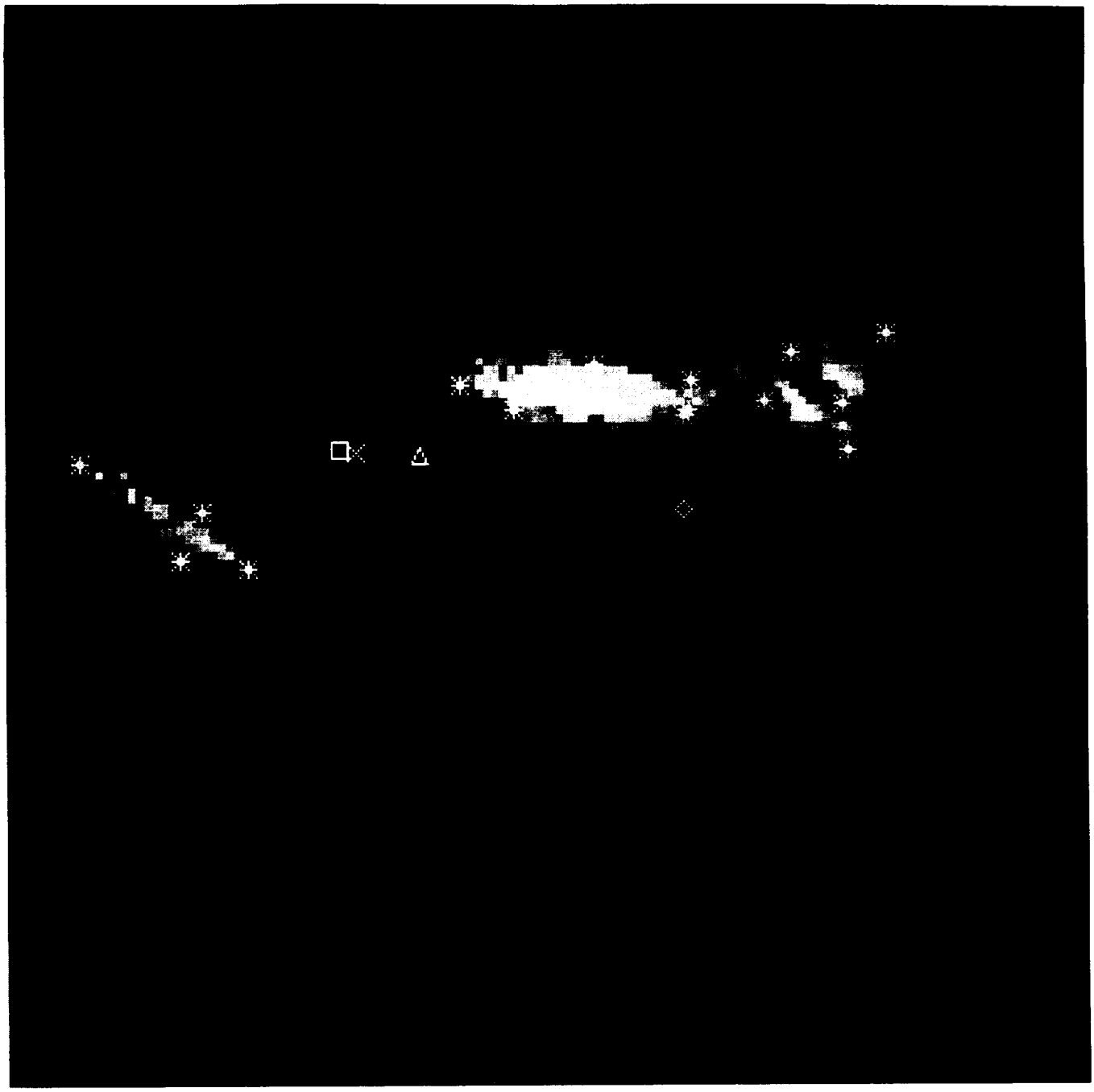

Figure 3c
Zoomed part of a backprojection of the later image (Figure 1 right side). For centering and marking see Figure 3a. The calculated position of Amalthea's footprint at 11:21 is marked by a square. The faint emission to the west of this square may be its real footprint.

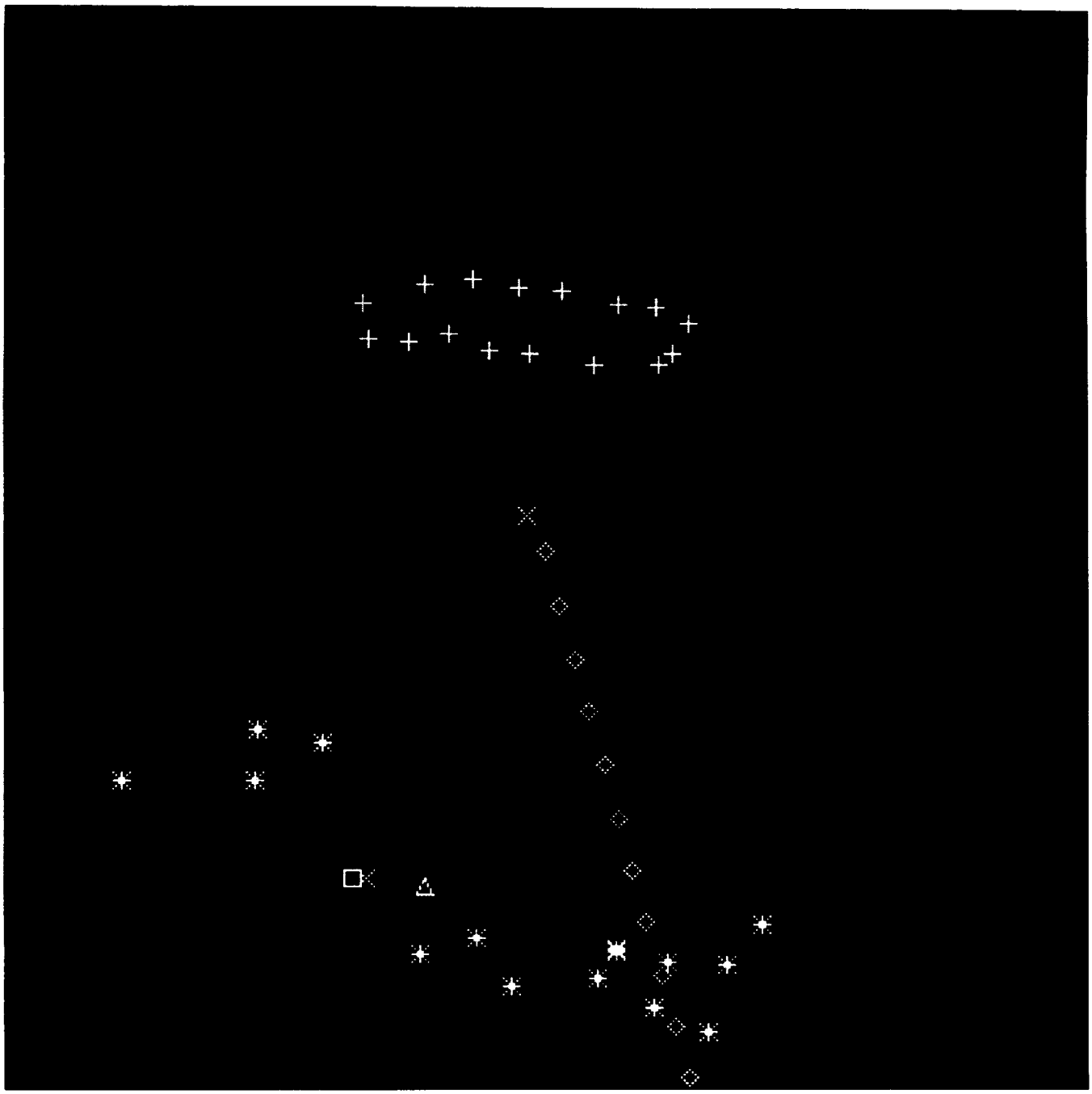

Figure 3d
Zoomed part of a backprojection of the later image (Figure 1 right side). For centering and marking see Figure 3b. The crosses correspond to those in Figure 3b and show approximately the earlier emission region S2.

Using the Nautical Almanac from 1994, we find Amalthea at longitudes between 275.2° (impact time) and 279.6° (47 minutes later). During these times, its footprint was approximately in the middle of the gap between the two northern hemispheric emissions, see Figure 3a and 3c. Note the faint emission just to the east of Amalthea's latest footprint marking (a square for 11:21 UT) in figure 3c. There is a possibility, that this is its footprint, but it does not differ very much from other granules seen in the global images, thus a positive identification is not possible. The hot spot seen by McGregor et al. (1996) is centered just south of region N1, we marked its location with a diamond.

We explore the second question by zooming the emission regions of both hemispheres, framing the northern ones by a couple of markings (stars in Figure 3a), and plotting footprints of the marks into the zoomed image of the southern ones (stars again); see Figure 3b. It seems, that region S2 can be split into two emission regions which roughly correspond in size and in shape to the regions N1' and N2', but with different offsets from their location: N2' is southwest of region S2 and projection N1' directly to the south. These subregions of S2 are slightly shifted to both sides from the ground projection of the incoming fragment's trajectory. The center of the rings observed by McGregor et al. (1996) is approximately in line with this projection. In Figures 3c and 3d, we applied the same framing and projection procedure to the image obtained 57 minutes after the impact. We get similar results for region S2 of this image: Here N1' is shifted to the south again, but N2' is more to the east than in Figure 3b.

Comparing Figures 3b and 3d, we also see the temporal evolution of the impact sites: The development of a darkened region, which is shifted to the left of the fragment trajectory. Region S1 (marked by crosses in Figure 3b) has faded, but the markings in Figure 3d (again crosses) show that it is located on the boundary of the dark region.

In Figure 4, we overplotted the later image with boundaries of regions N1 and N2 from the earlier image. Here, region N1 is shifted to the north, but its western part is smaller in latitude while its eastern part is washed out. Region N2 is shifted to the northwest and faded apart from a small stripe. Marks (triangle, x, square) show Amalthea's footprint wandering from the middle of the earlier emission regions at the time of the impact roughly to the middle of the emission regions in this image.

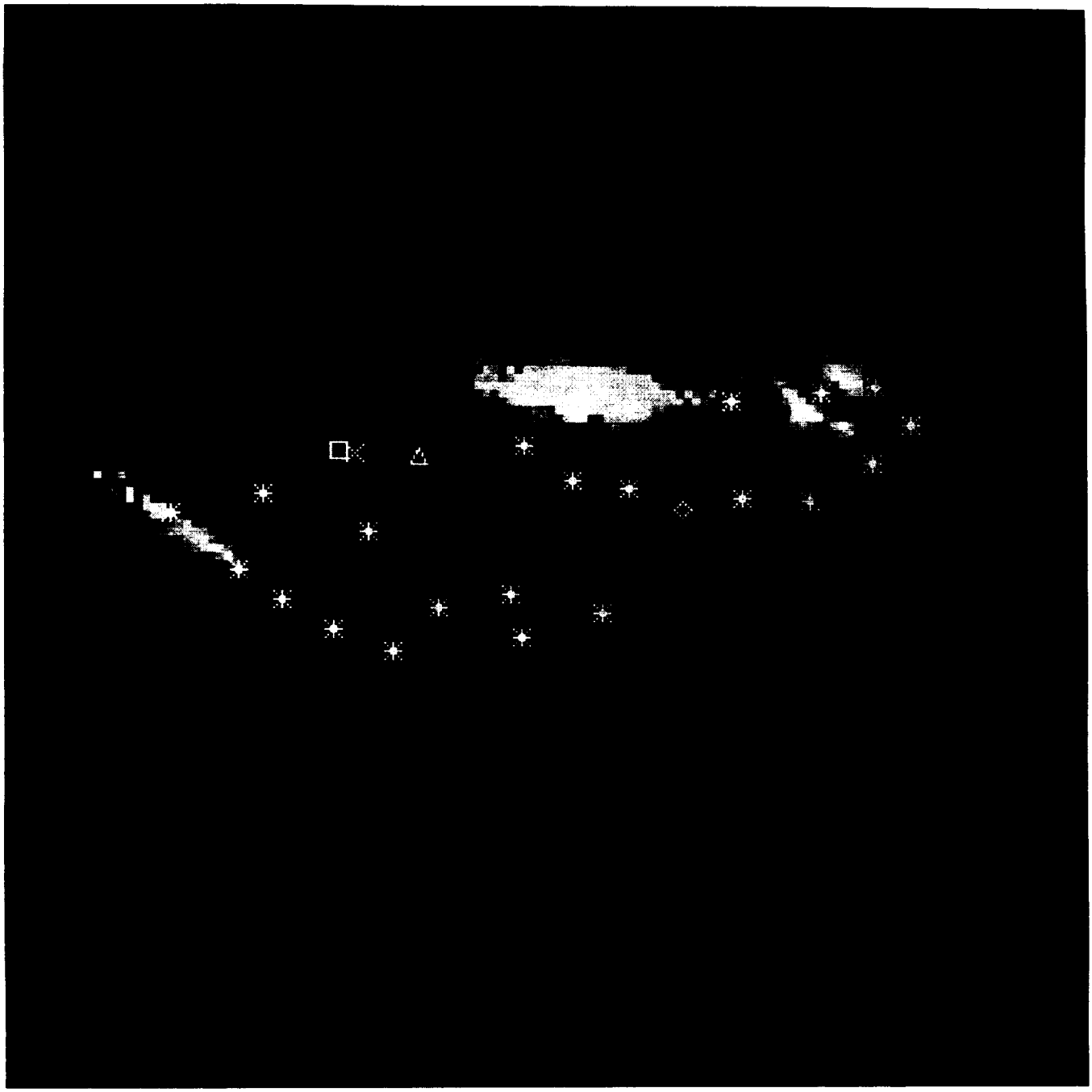

Figure 4
Northern emission regions of the later image in comparison to those in the earlier one, shown as stars. The positions of Amalthea's footprints are marked as before.

III.D Discussion

The following points will be discussed:

a) Relation of emissions to impact

b) Geometry of the southern emission regions.

c) Mapping of S2 to N1 and N2

d) Splitting of N1, N2. Absence of a conjugate emission region to S1

e) Brightness of N1, N2 relative to S1, temporal changes

f) New set of proposed mechanisms

a) From 112 images taken with the HST WFPC2 for a duration of more than 15 months these are the only two images which show mid-latitude far-UV emissions (Clarke et al., 1996). Thus, from the statistics, there is some evidence that these emissions are connected with the SL9 impact, but no certainty. The geometry of the emission regions at the impact site provides additional evidence due to their approximate ring shape and due to the southeast direction of the ring extension which is also the direction of the ejecta.

b) Figure 3b is comparable to figure 15 of McGregor et al. (1996) which shows (on the left side) a great ring with strong emission southeast of the impact location at about 11:40, 29 minutes later. By optical fitting of a circle to the bright emissions north and south of the impact location, we determined the ring center to be at -45.3 ± 0.2°, 279.7±0.2° and the ring radius to be 7500 ± 400 km. This approximates the 8000 km radius assumed by McGregor et al. (1996) as origin of their rings and it corresponds to the crescent region of Hammel et al. 1995 for the G impact, 7000 - 12500 km. In contrast, Figure 3d suggests that the FUV emission S2 is stationary, while S1 has faded away. The southeast border of the ring extension is at a distance of ~20100 km from the ring center. The more distant of the two bright subregions contained in S2 is about 15° to the east of the impact trajectory which is compatible with the Coriolis rotation of flying ejecta material relative to the planet (Boslough et al., 1995). Note, however, that our estimated ring center is northwest of the ring center determined by McGregor et al. (1996).

c) The similarities in shape and size of S2 and the magnetic mappings N1' and N2' give strong evidence, that these are real magnetic connections between both hemispheres. The operations (movements and rotations) necessary to cover S2 with the mappings of N1' and N2' differ. This suggests either a strong local anisotropy in the magnetic field (northern or southern hemisphere) or disturbances of the flux-tube geometry (or scattering of particles out of strict flux-tube confinement), the latter either spread along the whole flux-tube lengths or localized.

d) L values of region S1 are from 1.40 to 1.50 (O6 model : 1.39 to 1.44), those from region S2 are between 1.89 and 2.23 (1.91 and 2.43) and the L values of Amalthea are from 2.6 to 2.61 (2.61 to 2.62) for the earlier image. De Pater et al. (1997) suggest a dramatic change of the electron pitch angle distribution due to absorption and pitch angle scattering by Amalthea and absorption by the ring at L(O6) ~1.6 to 1.95:

Basically they show that the number of electrons with small pitch angles ($\alpha \leq \sim 60°$) is increased and the number of those with large pitch angles is decreased at Amalthea's orbit. A fraction of the inward diffusing electrons from greater L shells with $\alpha \leq 70°$ is assumed to be absorbed by Amalthea and the absence of high latitude synchrotron emission at L(O6) ≤ 2 is interpreted as strong absorption (90 %) of electrons with small pitch angles by the ring.

This model fits perfectly with our findings about the geometry of the far-UV emission regions and their magnetic mapping. A local disturbance of magnetic and electric fields by Amalthea may be responsible for a shift of region S2' to higher latitudes and perhaps also for its splitting into emission regions N1 and N2. Absorption by the ring explains the absence of a conjugate emission region to S2. At this stage, we are not confined to energetic electrons as the cause of far-UV emissions. The hot spot observed by McGregor et al. (1996) near to region N1 is compatible with H_3^+ emissions. McGregor et al. observed only one spot, but this spot was large, covering easily regions N1 and N2, as can be seen in Figure 11 (3.42 μm, 10:54:04 UT) and Figure 12 (3.99 μm, 10:59:45 UT) of their paper. Why is no splitting detectable in the infrared? First, these images have a lower resolution than the far-UV images. Second, infrared emission is of lower energy than far-UV emission, and energy cascading into an atmosphere is only weakly confined to the magnetic fieldlines of high energetic particles carrying it initially, especially if there are neutral particles as intermediate carriers which spread it into all directions.

e) The far-UV images were obtained after the main event, at a time, when the plume in the UV and optical images has fallen back and may have bounced several times (Mac Low, 1995). Each time it bounces back, it creates a shock which may be able to ionize particles and even to accelerate them, while a lot of energy is carried away by radiative cooling. According to numerical simulations, e.g., Boslough et al. (1995) we would (adding the bouncing effect) expect several emission regions southeast of the impact, roughly in line with the incoming fragment's trajectory, where the radiated energy should diminish with increasing distance to the center, resulting in smaller high energy emission regions. We would also expect that these high energy effects are of smaller duration than emissions at lower energies. Due to the long distance along the magnetic fieldlines,

there is a time delay for emissions created by energetic particles in the other hemisphere, thus emissions in the northern hemisphere would be brighter, reflecting the energies near to the impact region at earlier times. An additional contribution may be possible due to the nature of the disturbance from Amalthea, e.g., triggered pitch-angle diffusion of ambient energetic particles.

What causes Region S1? Zahnle (1996) explains that the velocity field of the plumes may be isotropic where material accelerated straight up has the highest velocities. This would account for the ring shaped crescent regions observed in HST images. It may be possible that isotropization occurs at lower energy levels whereas higher energy levels more reflect the impact geometry. Note, that the brightest part of region S1 is located in the continuation of the particle trajectory.

f) Hill and Dessler (1995) proposed that the "snowplow" effect of the impact plume is responsible for the emission S1 and that a Birkeland-current circuit driven by a dynamo effect causes the northern hemispheric emission regions. This model is not able to fully explain the observed emissions: There is some evidence from various three dimensional MHD-models, that the hottest region in a shock is located near to the symmetry line where an obstacle faces the incoming plasma, and this should also be the region where radiative cooling is strongest and thus most radiation is emitted. Second, there is no difference in the magnetic field strength between northern and southern emission regions which is able to account for the increased brightness of the northern hemispheric emissions. Brecht et al. (1995) proposed a shock acceleration process by an upward moving shock in order to explain the synchrotron radiation enhancement following the impacts. This mechanism works on short enough time scales to explain the appearance of highly energized ions within the time of the far-UV observations as well as at earlier times, e.g., for the IUE observations. In the latter case, the incoming particle cloud would be responsible for the emissions in the impact region, either directly on the trajectory or at its footprints observed at various altitudes, e.g., above the trajectory.

IV. Summary

We used an improved model of the magnetic field, a high time resolution calculation of the trajectory and refined images of the far-UV emission for a re-analysis of the fragment K impact as observed by the HST WFPC2 camera. We noted that the emission region around the impact site is shaped like a twice broken ring with an extension to the southeast, where emission maxima occurred roughly in line with the fragment trajectory. The distance of the ring is estimated as 7500 $\pm$ 400 km and its location at -45.3 $\pm$ 0.2°, 279.7 $\pm$ 0.2°, northwest from a ring center observed by McGregor et al. (1996). The southeast extension of the ring consists of two bright subregions west

and (the more distant one) east from the down projected trajectory. These subregions are compatible in size and shape with magnetically projected emission regions on the northern hemisphere, but the projections are located more to the west and to the south. It turns out that Amalthea's footprint is located in the gap between the northern hemispheric emissions at the time of the impact as well as during the imaging. Supporting suggestions of de Pater et al. (1997), we conclude that Amalthea may cause a disturbance in Jupiter's magnetic and electric field that leads in this case to scattering of particles onto field lines at higher latitudes. The ring located just inside Amalthea's orbit possibly absorbed energetic particles coming from the emission region north of the impact. The shock acceleration mechanism of Brecht et al. (1995) seems feasible to explain the existence of the emission regions in the northern hemisphere if we assume that the plume provides enough energy at its second bounce.

In conclusion, once the observational basis of originally proposed numerical simulation study was found to be substantially different than had been believed (in published papers at the time), it was clear that a different, but equally illuminating course of study had to be taken. That is, to embark on a study of ill-posed hypotheses, is not a reasonable course of action. Our careful study of the auroral emissions with a newly developed code which combines the latest Jupiter magnetic field model with projection geometry capability has in fact permitted us to be able to eliminate some proposed mechanisms and to point to a new scenario which appears to satisfy the observational evidence. We will shortly submit the results of this study for publication. Because we have gone beyond the end of the funded project, the paper will be submitted to *Icarus* which has no page charges.

V. Acknowledgments

In addition to obvious support of this work by this NASA grant (NASW-4797), we wish to acknowledge the important contributions of P. Chodas who provided the latest revised comet orbital trajectories, and J. Connerney who provided us with his latest Jupiter magnetic field model results before publication.

VI. References

Ballester, G., W. M. Harris, G. R. Gladstone, J. T. Clarke, R. Prangé, P. D. Feldman, M. R. Combi, C. Emerich, D. F. Strobel, A. Talavera, S. A. Budzien, M. B. Vincent, T. A. Livengood, K. L. Jessup, M. A. McGrath, D. T. Hall, J. M. Ajello, L. ben Jaffel, D. Rego, G. Fireman, L. Woodney, S. Miller, and X. Liu 1995. Far-ultraviolet Emissions from the

Impact Sites of Comet P/Shoemaker-Levy 9 with Jupiter, *Geophys. Res. Let.* **22**, 2425 - 2428, 1995.

Baron, R., R. D. Joseph, T. Owen, J. Tennyson, S. Miller, and G. E. Ballester, Imaging Jupiter's aurorae from H_3^+ emissions in the 3 - 4 μm band. *Nature* , **353**, 539 - 542, 1991.

Boslough, M.B., D.A. Crawford, A.C. Robinson and T.G. Trucano, Mass andpenetration depth of Shoemaker-Levy 9 fragments form time-resolved photometry, *Geophys. Res. Lett.*, **21**, 1555, 1994.

Brecht, S. H., M. Pesses, j. G. Lyon, N. T. Gladd, S. W. McDonald 1995. An explanation of synchrotron radiation enhancement following the impact of Shoemaker-Levy 9 with Jupiter. *Geophys. Res. Let.*, **22**, 1805 - 1808.

Clarke, J.T., L.B. Jaffel, A. Vidal-Madjar, G.R. Gladstone, J.H. Waite, Jr., R. Prange, J.C. Gerard, J. Ajello, and G. James, HST/GHRS H_2 Rotational Spectra of Jupiter's Aurora, *Astrophys. J. Lett.*, **430**, L73, 1994.

Clarke, J.T., R. Prangé, G. E. Ballester, J. Trauger, R. Evans, D. Rego, K. Stapelfeldt, W. Ip, J.-C. Gérard, H. Hammel, M. Ballav, L. B. Jaffel, J.-L. Bertaux, D. Crisp, C. Emmerich, W. Harris, M. Horanyi, S. Miller, A. Storrs, and H. Weaver Hubble Space Telescope Far-Ultraviolet Imaging of Jupiter during the Impacts of Comet Shoemaker-Levy 9, *Science* , **267**, 1302, 1995.

Chevalier, R.A and C.L Sarazin, Explosions of infalling comets in Jupiter's atmosphere, *Astrophys. J.*, **429**, 863, 1994.

Connerney, J. E. P., The magnetic field of Jupiter: A generalized inverse approach. *J. Geophys. Res.*, **86**, 7679 - 7693, 1981.

Connerney, J. E. P. Doing more with Jupiter's magnetic field, in *Planetary Radio Emissions III*, eds. S. J. Bauer and H. Rucker, Austrian Academy of Science, Austria, 13 - 33, 1995.

Connerney, J. E. P., R. Baron, T. Satoh, and T. Owen, Images of excited H_3^+ at the foot of the IO flux tube in Jupiter's atmosphere. *Science*, **262**, 1035 - 1038, 1993.

Connerney, J. E. P., M. H. Acuna, N. F. Ness, and T. Satoh, New models of Jupiter's magnetic field constrained buy the Io flux tube footprint. *To be published*, 1997.

Cravens, T.E. Comet Shoemaker-Levy 9 Impact with Jupiter: Aeronomical Predictions, *Geophys. Res. Let.* **21**, 1075, 1994.

De Pater, I., M. Schulz, and S. H. Brecht, Synchrotron evidence for Amalthea's influence on Jupiter's electron radiation belt. J. Geophys. Res., **102**, 22043 - 22064, 1997.

Dessler, A.J. and T.W. Hill, Some Interactions between Dust from Comet Shoemaker-Levy 9 and Jupiter, *Geophys. Res. Let.*, **21**, 1043, 1994a.

Dessler, A. J., and T. W. Hill, *Bull. Am. Astron. Soc.*, **26**, 1593, 1994b.

Gerard, J.C., D. Grodent, R. Prange, J.H. Waite, Jr., G.R. Gladstone, V. Dols, F. Paresce, A. Storrs, L. Ben Jaffel, and K.A. Franke, A Remarkable Auroral Event on Jupiter Observed in Ultraviolet with the Hubble Space Telescope, *Science*, **266**, 1675, 1994.

Gombosi, T. I, and A. F. Nagy, Time-dependent modeling of field-aligned current-generated ion transients in the polar wind, *J. Geophys. Res.*, **94**, 359, 1989.

Hammel, H. B., R. F. Beebe, A. P. Ingersoll, G. S. Orton, J. R. Mills, A. A. Simon, P. Chodas, J. T. Clarke, E. de Jong, T. E. Dowling, J. Harrington, L. F. Huber, E. Karkoschka, C. M. Santori, A. Toigo, D. Yeomans, R. A. West, HST Imaging of atmospheric phenomena created by the impact of comet Shoemaker-Levy 9. *Science*, **267**, 1288 - 1296, 1995.

Hill, T. W., and A. J. Dessler, Mid-latitude Jovian Aurorae produced by the impact of comet Shoemaker-Levy 9. *Geophys. Res. Let.*, **22**, 1817 - 1820, 1995.

Kellogg, P.K., Plasma effects on the interaction of a comet with Jupiter, *Geophys. Res. Letters*, **21**, 1055, 1994.

Kim, S. J., P. Drossart, J. Caldwell, J.-P. Maillard, T. Herbst, and M. Shure, Images of aurorae on Jupiter from H_3^+ emission at 4 μm. *Nature*, **353**, 536 - 539, 1991.

Mac Low, M.-M., Entry and fireball models vs. obserations: What have we learned? , in *The Collision of Comet Shoemaker-Levy 9 and Jupiter*, edited by K.S. Noll, H.A. Weaver, and P.D. Feldman, Space Telescope Science Series No. 9, Cambride University Press, pp. 157-182, Cambridge, 1996.

McGregor, P. J., P. D. Nichelson, and M. G. Allen, CASPIR observations of the collision of comet Shoemaker-Levy 9 with Jupiter. *Icarus*, **121**, 361 - 388, 1996.

Miller, R.H. and M.R. Combi. A Coulomb Collision Algorithm for Weighted Particle Simulations. *Geophys. Res. Lett.* , **21**, 1735-1738, 1994.

Miller, R. H., C. Rasmussen, M. Combi, T. Gombosi, D. Winske . 1995 Ponderomotive acceleration in the Auroral Region: A Kinetic Simulation. *J. Geophys. Res.*, **100**, 23901-23916, 1995.

Miller, S., N. Achilleos, B.M. Dinelli, H.A. Lam, J. Tennyson, M.-F. Jagod, T.R. Geballe, L.M. Trafton, R.D. Joseph, G.E. Ballester, K. Baines, T.Y. Brooke, G. Orton, The effect of the impact of Comet Shoemaker Levy-9 on Jupiter's Aurorae, *Geophys. Res. Lett.*, **22**, 1629,1632, 1995.

Prangé R., I.M. Engle, J.T. Clarke, M. Dunlop, G.E. Ballester, W.H. Ip, S. Maurice, J. Trauger, Auroral Signature of Comet Shoemaker-Levy 9 in the Jovian Magnetosphere, *Science*, **267**, 1317, 1995

Waite, Jr., J.H., F. Bagenal, F. Seward, C. Na, G.R. Gladstone, T.E. Cravens, K.C. Hurley, J.T. CLarke, R. Elsner, and S.A. Stern, ROSAT Observations of the Jupiter Aurora, *J. Geophys. Res.*, **99**, 14799, 1994.

Waite, Jr., J.H., G.R. Gladstone, K.A. Franke, W.S. Lewis, A.C. Fabian, W.N. Brandt, C. Na, F. Haberl, J.T. Clarke, K.C. Hurley, M. Sommer, and S. Bolton, ROSAT Observations of X.ray Emissions from Jupiter during the Impact of Comet Shoemaker-Levy 9, *Science*, **268**, 1598-1601, 1995.

Watanabe, J., T. Yamashita, H. Hasegawa, S. Takeuchi, M. Abe, Y. Hirota, E. Nishihara, S. Okumura, and A. Mori, Near-IR observation of cometary impacts to Jupiter: Brightness variation of the impact plume of fragment K. *Publ. Astron. Soc. Jpn.*, **47**, L21 - L24, 1995.

Zahnle, K., Dynamics and chemistry of SL9 plumes, in *The Collision of Comet Shoemaker-Levy 9 and Jupiter*, edited by K.S. Noll, H.A. Weaver, and P.D. Feldman, Space Telescope Science Series No. 9, Cambride University Press, pp. 183-212, Cambridge, 1996.